Electronic Differential Design for a Vehicle with Four Independently Controlled In-wheel Motors

Amin Hajihosseinlu, Shaahin Filizadeh, Garry Bistyak, Erwin Dirks
Dept. of Electrical and Computer Eng.
University of Manitoba
Winnipeg, Canada

***Abstract*—In this paper a simple topology for electronic differential in an electric vehicle with four independent In-wheel motors is proposed. Based on inputs of the steering wheel angle and the acceleration pedal position, this method uses real-time power management and produces different torque references for the four wheels and, consequently the angular velocity of each wheel will be adjusted. Using slip-ratio calculations the proposed algorithm extracts maximum output torque by optimizing the operating-point slip ratio. The paper also highlights an application of deployed in-wheel motors in yaw stability and suggests a simple yaw control strategy. The proposed electronic differential method is first investigated using MATLAB and is then implemented on a real-time digital simulator, which is then connected to a small motor to verify its performance in a hardware-in-loop scheme.**

I. INTRODUCTION

Environmental concerns along with the shortage and the uncertainty of the supply of fossil fuels have led the automotive industry to increasingly consider alternative vehicular drivetrains, such as hybrid, plug-in hybrid, and electric. Studies show that with improvements in batteries, electric motor drives, and power electronics, these environmentally friendly vehicles are able to perform satisfactorily and at times even better than conventional vehicles. In more-electric vehicles certain mechanical components are replaced with electric or electronic components that perform the same task. In an electric vehicle (EV), conventional (mechanical) differential must be replaced with an electric differential (ED), which performs the task of adjusting the torque applied to each wheel based on the present driving conditions. A well-designed electronic differential can make the vehicle both lighter and more stable in handling. Electric vehicles are expected to have faster torque response than conventional vehicles due to advanced motor-control methods (e.g., direct torque control), which allows the motor to generate rapidly varying amounts of torque. Use of regenerative braking enables the kinetic energy in the moving vehicle to be recuperated in the battery during braking periods, thereby increasing the efficiency of the drivetrain [1]. Different electric motors with high negative and positive torque characteristics have been investigated including switched reluctance and permanent-magnet synchronous motors [2], [3]. Drive-train layouts including one, two or four independently controlled motors have been considered. Use of four independent in-wheel motors provides the opportunity to generate different torque (speed) references to each wheel independently; this not only leads to better differential operation, but also has considerable potential for improved yaw-motion stability control [4]. In-wheel motor controllers have been considered for various aspects of motion stability such as yaw control, lateral control, and anti-skid braking systems [5]-[8]. Different topologies and aspects of electronic differential, such as master-slave control or synchronization structure, and sliding mode yaw motion control, have been investigated in the literature. In [9], the authors investigate the advantages of the ED in vehicle motion stability. Chen and Wang investigate an over-actuated ground electric differential with four independent In-wheel motors in [10]. This paper proposes an ED based on solid and provable geometric expressions, which describe the motion of the vehicle and its four wheels in a turn. Using a purely mathematical procedure in section II, the paper shows that addition of an ED requires simple modifications to the existing electric vehicle drive-train controller structure. Additionally the method proposed herein considers the slippage of the wheels in the design of the ED and proposes a novel method of yaw motion stability. In some parts of this paper it is assumed that the yaw rate and the ground vehicle speed are available through continuous sensing. Ground speed sensors using optical means are found in [11], [12]. Other speed estimation methods have also been proposed in the literature including in [13]. The paper continues with an introduction to ED and its necessity. Basic geometric equations that underline the turning action are then presented and used to derive a controller that generates different power commands for different wheels during cornering. In section III an algorithm for operation at optimal wheel slippage is developed using curves of adhesion friction versus wheel slippage. This allows for maximizing the traction force without excessive power consumption by each motor. In section IV, the action of the ED in preventing over- and under-steering and in increasing stability is discussed. Computer simulation and experimental results of the proposed methods are also given followed by conclusions

II. MATHEMATICAL MODEL DEVELOPMENT

In this section the mathematical model of a vehicle during turning is developed. This model will be used to design and develop an ED as will be described later in this section. The model is valid for front, back, and all-wheel electronic differential.

978-1-4799-6075-0/14/$31.00

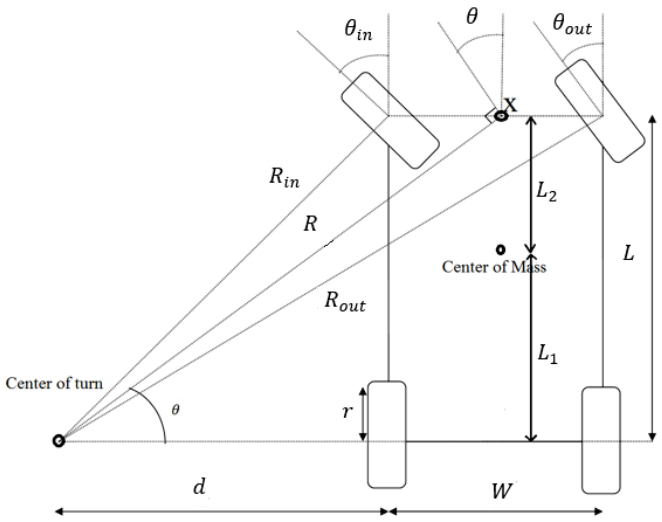

Fig. 1: Vehicle geometry

A. Geometry of turning

Fig. 1 shows the geometry of a vehicle during cornering. The ground speed of the center of each wheel can be obtained based on the vehicle ground speed (measured at point X in Fig. 1). The following equations show the ground speed of each wheel as a function of the ground speed (V) at point X, and the geometric parameters of the turn.

$$\begin{aligned} V_{lf} &= \frac{R_{in}}{R}V,\ V_{rf} = \frac{R_{out}}{R}V \\ V_{lr} &= \frac{d}{R}V,\ V_{rr} = \frac{(d+W)}{R}V \end{aligned} \tag{1}$$

The linear speed of the wheel (measured at its outer periphery) and its angular velocity are as shown in (2).

$$\omega_i = \frac{V_{w_i}}{r} \qquad i = lf, rf, lr, rr \tag{2}$$

where ω_i and V_{w_i} are angular and linear speed of each wheel, r is radius of wheels and lf, rf, lr, rr stand for left front, right front, left rear and right rear, respectively.

It is necessary to notice the difference between V_{w_i} and V_i as shown in Fig.2.
Expressions for ω_i can be obtained in terms of the vehicle ground speed, V, and other parameters. Note that

$$d = \frac{L}{\tan\theta} - \frac{W}{2} \tag{3}$$

where θ is the steering wheel angle. Since θ is measured continuously, the real time value of d is available. Therefore, using geometric equations R_{out}, R_{in}, R can be obtained. Subsequently,

$$\omega_i = f_i(\theta)V \tag{4}$$

This equation is valid if there is no wheel slippage; with consideration of the wheel slippage, this must be modified, as will be shown in section III.

Fig. 2 shows an overall configuration of the proposed topology. ED algorithm is implemented in the function block containing four equations including $F_1(\theta), F_2(\theta), F_3(\theta)$ and $F_4(\theta)$. Field oriented control method is used in this proposed algorithm.

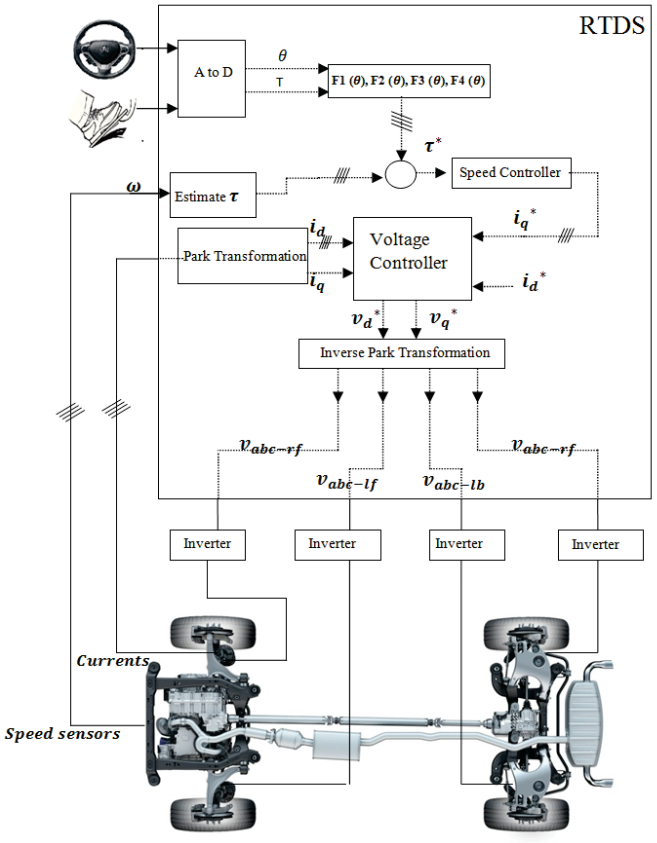

Fig. 2: Overall configuration of the model

B. Vehicle dynamic equations

Dynamic equations of the vehicle are divided in two parts. The dynamic equations of the four wheels are presented first, followed by the dynamic equations of the vehicle motion. The following shows the dynamics of the wheels, assuming that each wheel is powered by its own motor (in-wheel installation).

$$J\frac{d\,\omega_i}{dt} = \tau_i - Fr_i - b\,\omega_i \qquad i = lf, rf, lr, rr \tag{5}$$

where J is moment of inertia of each wheel, τ_i is the torque generated by the respective motor, Fr_i is rolling force of each wheel (see (6)) and b is the viscous friction coefficient.

$$Fr_i = U(S_i)N_i\cos(\alpha) \qquad i = lf, rf, lr, rr \tag{6}$$

In (6) S_i is the slip ratio of the particular wheel, U is the adhesion friction, which is function of wheel slippage, N_i is the normal force and alpha is the road slope angle. Fig. 3 shows typical $U(S_i)$ curves for various road surfaces. Slippage is defined as follows

$$S_i = \frac{V_{w_i} - V_i}{Max(V_{w_i}, V_i)} \qquad i = lf, rf, lr, rr \qquad (7)$$

Under normal conditions the slippage ratio is normally small and remains below 10%. Equation (8) shows the dynamic equation of the vehicle, derived as per Newtons second law of motion.

$$M\frac{dV}{dt} = \Sigma Fr_i - Fa \qquad i = lf, rf, lr, rr \qquad (8)$$

where M is vehicle mass and Fa is air drag which is shown in equation (9)

$$Fa = \frac{1}{2} C_d \rho V^2 \qquad (9)$$

where C is the drag factor (a function of the vehicle geometry and the frontal area of the vehicle), and ρ is the air density.

III. Inclusion of wheel slippage

When a vehicle moves on the surface of a road, the wheels may turn at a certain angular velocity; however the actual linear velocity of the vehicle may be somewhat lower. This is due to the slippage of the wheels, which does not fully translate to forward motion of the vehicle. In extreme cases, the vehicle may remain stationary while its wheels spin in place. The tire friction model introduced by Burckhardt has been used in this paper. It provides the tire-road coefficient of friction as a function of the wheel slip, S_i and the vehicle linear speed, V_x.

$$U(S_i, V_x) = [C_1(1 - e^{-C_2 S_i}) - C_3 S_i] e^{-C_4 S_i V_x} \qquad (10)$$

Slippage can be positive and negative. It is positive during acceleration and negative during deceleration (braking). The slippage curves during deceleration are obtained by odd symmetry of rules of the curves shown in Fig. 4. During acceleration $max(V_{w_i}, V_i)$ will be V_{w_i} and ΣFr_i in equation (8) will be positive to help the vehicle accelerate. Equation (11) evaluate slip by measuring steering wheel angle, vehicle speed and angular velocity of each wheel.

$$S_i(t) = 1 - \frac{V_i(t)}{V_{w_i}(t)} = 1 - \frac{V.f_i(\theta)}{V_{w_i}(t)} \qquad (11)$$

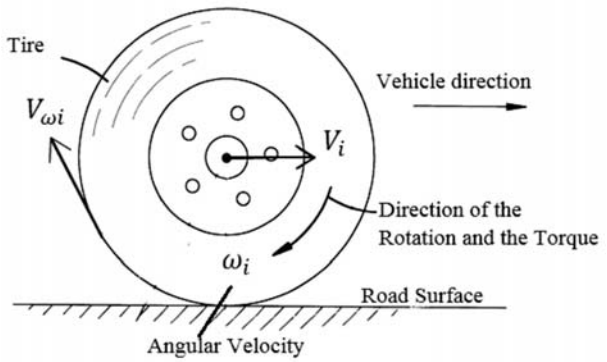

Fig. 3: Wheel and related parameters

As it is seen in Fig. 3, V_{w_i} and V_i are different because of slippage. Considering the above, there will be four independent slip ratios for the four wheels. They are called s_{lf}, s_{rf}, s_{lr} and s_{rr} which are slip ratio of left front, right front, left rear and right rear wheels, respectively. As an example for wheel left front, during the acceleration $Max(Vw_{lf}(t), V_{lf}(t))$ is equal to $Vw_{lf}(t)$ and ,on the other hand, during deceleration $Max(Vw_{lf}(t), V_{lf}(t))$ is equal $V_{lf}(t)$. In first case both slip and adhesion coefficient are positive, so the waveforms are in first quadrant. In the second case, however, both the slip and the adhesion coefficient are negative, i.e., the waveforms are in third quadrant. The curves in Fig. 4 are obtained using (10) with parameter values listed in Table 1. C_4 is equal to 0.04. Given the curves in Fig. 4 one can maximize the output torque to each wheel while the consumed power by each motor is minimized. The main goal is to keep the slip ratio in the stable regions. The stable region is the rising side of the curves in Fig. 4, before the adhesion coefficient reaches its maximum; beyond this point, the slippage becomes uncontrollably high while the adhesion coefficient drops rapidly.

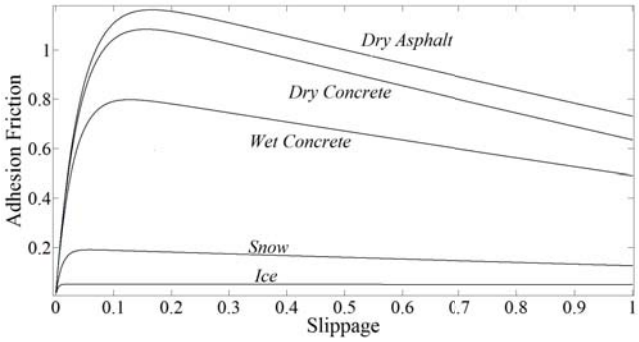

Fig. 4: Adhesion coefficient versus slip ratio for different road conditions

TABLE I: Burckhardt friction model parameters

Surface Condition	C_1	C_2	C_3
Dry asphalt	1.2801	23.99	0.52
Wet asphalt	0.857	33.822	0.347
Dry concrete	1.1973	25.168	0.5373
Snow	0.1946	94 .129	0.0646
Ice	0.05	306.39	0

Fig. 5 shows the slippage characteristics as a function of the vehicle speed for motion of the vehicle on dry asphalt. As seen from the figure, the maximum adhesion coefficient occurs at different values of the slip ratio for different values of the vehicle speed. Fig. 6 shows the slip ratio that corresponds to the maximum adhesion coefficient as a function of the vehicle speed. Therefore, using a look-up table one can command the slip ratio that gives the maximum adhesion coefficient for different vehicle speed. With this notion, one can re-write (4) as follows explicitly as a function of the slip ratio.

$$\omega_{lf} = (1 + s_{lf}) f_1(\theta) V \tag{12a}$$
$$\omega_{rf} = (1 + s_{rf}) f_2(\theta) V \tag{12b}$$
$$\omega_{rb} = (1 + s_{lr}) f_3(\theta) V \tag{12c}$$
$$\omega_{lb} = (1 + s_{rr}) f_4(\theta) V \tag{12d}$$

Note that these equations are the modified versions of the angular velocity in (4) with inclusion of the wheel slip. It is expected that with the inclusion of the slip, the angular velocity of the wheels be higher that what is predicted using (4).

IV. Yaw motion control

A method for improvement of yaw motion stability of the vehicle is proposed as follows. First, parameters of the motion, namely, $\theta, T, \gamma, \omega_i, V$, are measured. The slip ratio of each wheel is then calculated using (7). The desired yaw rate must also be evaluated based on steering wheel angle (θ) and the vehicle speed (V) using (13).

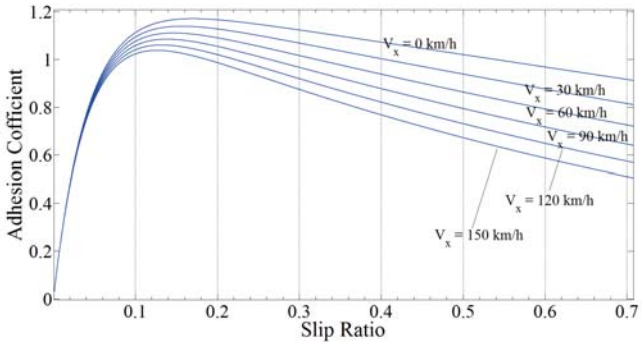

Fig. 5: Adhesion friction versus slippage for different vehicle speeds

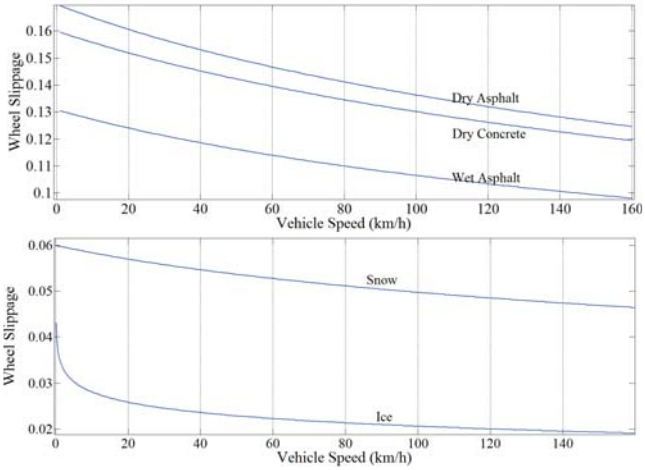

Fig. 6: Wheel slippage corresponding to the maximum adhesion friction for different types of road

The actual yaw rate is then compared with this desired value to determine if corrective action is necessary.

$$\gamma = L_1 . V \sin(\theta) \tag{13}$$

To implement the propose yaw motion stability algorithm, the maximum slippage needs to be determined using a look-up table, extracted form Fig. 6, which is a function of the vehicle speed and the road type. The four calculated slip ratios are tracked with a high-speed processor; by adjusting the reference torque to each wheel the yaw motion control algorithm forces the slip ratios to remain below the optimum. If the slippage of a wheel exceeds the optimum, the algorithm reduces the torque command to that wheel to reduce the slippage to below the optimum, and increases the torque command(s) to the wheel(s) with the lowest slip ratio. Yaw rate is considered positive if the vehicle turns counterclockwise and vice versa. Following flowchart simply provides a better view of the proposed yaw motion control. First, the information about current slippage status for individual wheels is needed. Information from Fig. 6 will provide the optimal slip ratio which generate maximum torque. Torque capacity (TC) is defined as the difference between the torque that keeps the slippage at the optimum point and the current instantaneous torque command. In this proposed control strategy, the instantaneous torque command will never be allowed to exceed the optimum torque. As seen in Fig. 7, yaw rate error must be obtained. This error is the difference between measured yaw rate and desired yaw rate. A positive yaw rate error is over-steer in the counterclockwise direction. This means that the compensating yaw force must be clockwise. Therefore, torque will be added to the left wheels taking into account the torque capacity of the left wheels. If the torque capacities of either of the left wheels is close to zero, i.e. the instantaneous torque command is already close the maximum possible torque, then torque will not be changed in that wheel. At the same time, the torque commands will be reduced to the right wheels especially the one with lower torque capacity. By using this strategy, firstly the yaw

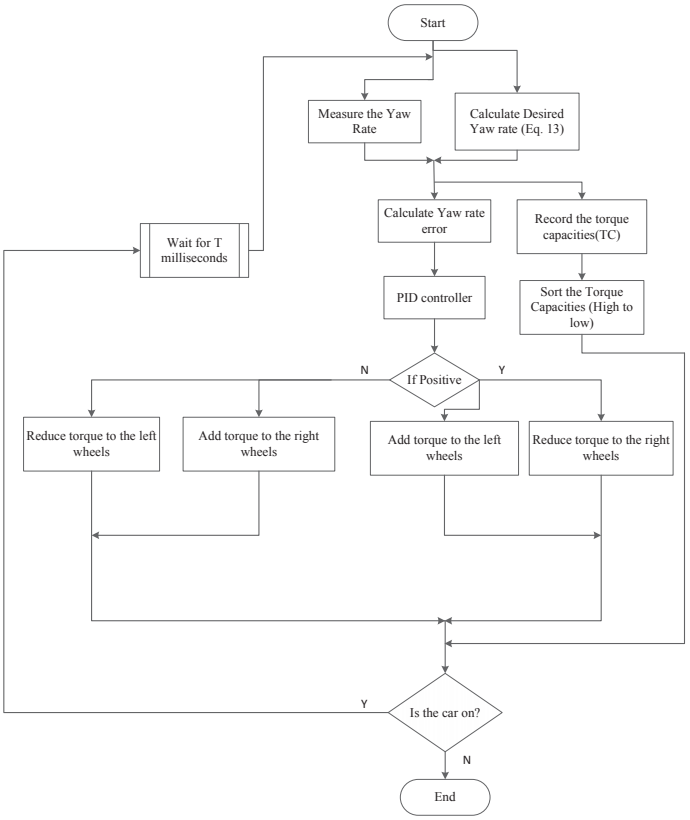

Fig. 7: Yaw motion control strategy flow chart

compensation will be very fast due to the quick response of the four electric motors. Secondly, The torque capacities of all wheels tend to be close to each other and in the stable region. In the same way, if the yaw rate error is negative, the inverse strategy will be applied.

V. Modeling and Simulation Results

A detailed computer model of a vehicle is developed and implemented (in MATLAB) to simulate the functionality of the proposed electronic differential. The parameters of the vehicle required for this are given in Table 1; these parameters pertain to a large all-terrain vehicle (ATV). The simulations are conducted for motion on dry asphalt on a flat road. The two inputs to the model, i.e., the steering wheel angle and the traction force, are shown in Fig. 8(a) and (b), respectively. The latter is an indication of the command given by pressing the acceleration pedal. As explained in Section II, the command given by the acceleration pedal is used by the developed ED to generate four independent torque reference values to each wheel. The wheel speed increases and causes a slight increase in slip ratio (see (7)), thereby increasing the rolling force (via (6)); the increasing rolling force increases the vehicle speed (as in (5)).Fig. 9a shows four torque references for four wheels and as it is seen, when steering wheel angle increases the four speed will have different values. Fig. 9b shows the angular speed of wheels, they follow the torque command very well. Fig. 9c shows the slippage of each wheel. It is seen that as the torque command increases the average slip ratio will increase. Finally, vehicle speed will be the respond to summation of four different torque on four wheels.

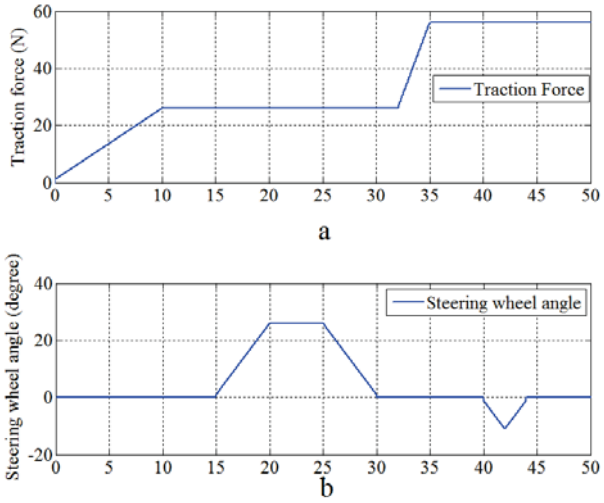

Fig. 8: Simulation results (inputs)

VI. Experimental Verification of Electric Differential

The simulation results in Section V showed the response of the developed ED algorithm to the commands of steering wheel angle and traction force. In reality, the torque commands generated by the ED algorithm are transmitted to individual electric motor drive systems (for each wheel), which then apply suitable voltages and currents to their respective motor to achieve the commanded torque. The dynamics of the electric motor drive system was ignored in the simulation results presented earlier. In this section a small-scale laboratory setup is developed to test the performance of the proposed algorithm using an actual electric motor drive system connected to a synchronous machine, which emulates the in-wheel motor in the actual implementation of the system in a real vehicle. The ED algorithm is implemented on a real-time simulator (RTDS), which is then interfaced with the power electronics of the drive system. A field-oriented control scheme is developed, which upon receiving the torque command from the RTDS will generate proper stator current commands for the ensuing PWM switching scheme. The synchronous motor (with constant field current) responds by exerting the requested amount of torque on its shaft. Fig.10 (a) shows the acceleration pedal and steering wheel (input variables). Four different torque references are shown in Fig.10(b). Although the motors are not connected to an actual vehicle, two flywheels are attached to the shafts in order to resemble the loading on the motor similar to a real vehicle.

TABLE II: Vehicle geometric parameters

Vehicle Length	1.94 m	Width	1.27 m
Mass	1200 kg	Wheel radius	0.3175 m
Wheel moment of inertia	1	Steering wheel gear	20
Air drag coefficient	2		

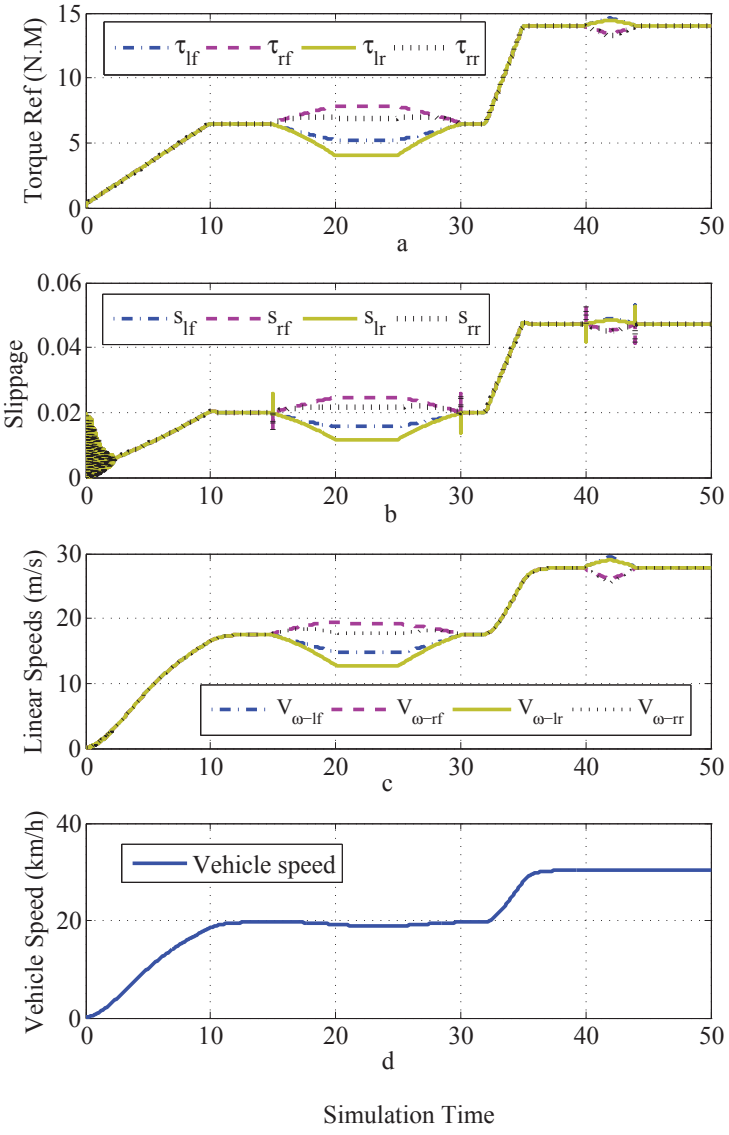

Fig. 9: Simulation results (outputs)

The comprehensive simulation model developed in MATLAB uses two dependent dynamic models, i.e., the wheel and the vehicle dynamic models (equations (5) and (8)). In the experimental setup the motors are not connected to an actual vehicle; however, using two flywheels with specific inertia and viscous friction values, it properly resembles a real vehicle model and, therefore, it can be used to verify the ED algorithm.

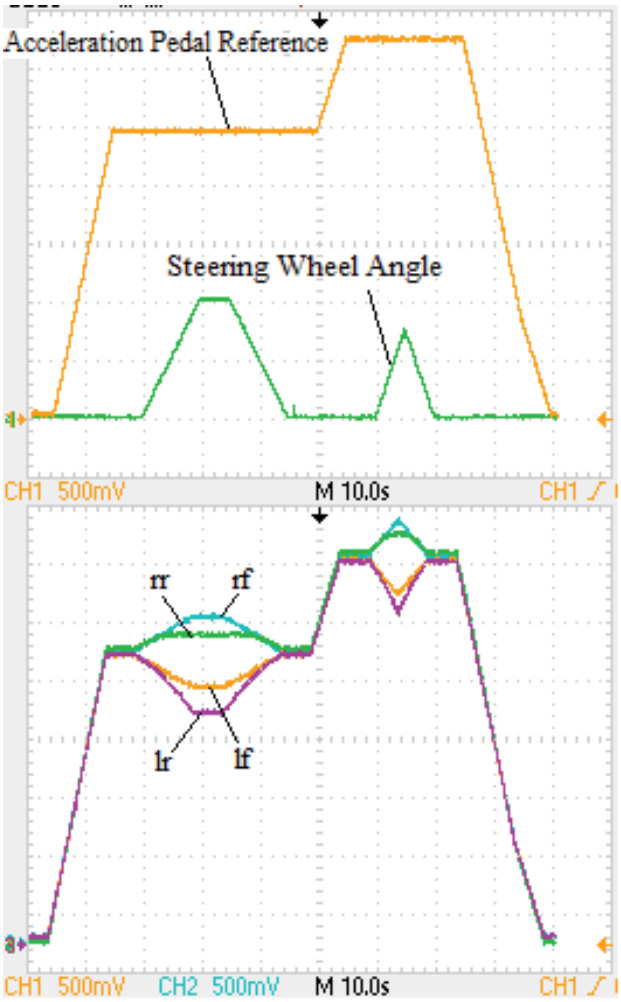

Fig. 10: Experimental results a) Speed reference and steering wheel angle (inputs) b) Four different speed references of the motors

Fig. 11 shows the torque (speed) reference and the speed response of the car. Since the effect of wind and road grade are neglected (no load), the speed reference is linearly proportional to the force reference. This figure also illustrates the performance of the motor drive setup. As it is seen, the speed response of the motor is fast and closely follows the command.

Fig. 12 shows two flywheels. Since the experiment is not performed in a real vehicle, the proposed yaw motion control method (section IV) cannot be tested in this setup. In order to experiment the proposed yaw motion control algorithm, one can use a lookup table extracted from Fig. 6 to optimize the torque reference values given to the motors. A dynamometer with capability to exert different forces on the four wheels is also needed to accomplish this test.

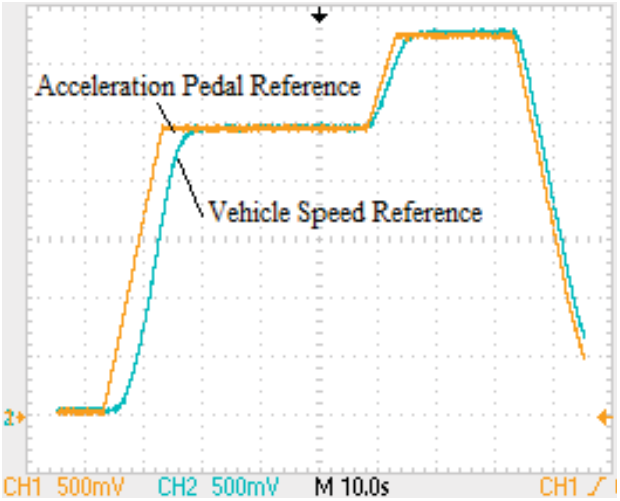

Fig. 11: Vehicle Speed(acceleration pedal) reference and Vehicle Speed

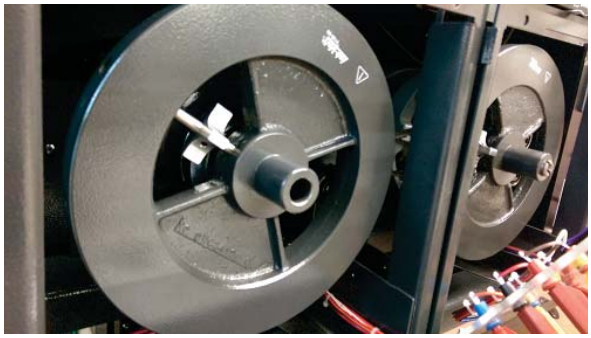

Fig. 12: Flywheels are connected to motor and dynamo-meter

VII. Conclusion

The paper presented a geometrically rooted algorithm for an electronic differential of a vehicle with four independently controlled wheels. The algorithm uses the steering wheel angle and the ground speed as its inputs, and generates torque commands for the four wheels. It was shown that with consideration of the slip ratio the electronic differential will improve the yaw motion stability as well. One of the issues in this scheme is that the available adhesion friction curves versus slippage is not very accurate. Therefore, this method may result in errors when the road condition suddenly changes. Further improvement may be needed to keep the slippage at the optimum operating point even with changing road conditions. Experimental results verified the performance of the developed algorithm in its independent differential model, although the limitations of the setup did not allow testing of the yaw motion stability features.

References

[1] S. R. Cikanek and K. E. Bailey, "Regenerative braking system for a hybrid electric vehicle," oct 2 2003, uS Patent 20,030,184,152.

[2] A. Hajihosseinlu, M. Jahanmahin, E. Afjei, and S. Tajik, "A novel four layer switch reluctance motor with high torque and ripple reduction," in *Power Electronics and Drive Systems Technology (PEDSTC), 2012 3rd*. IEEE, 2012, pp. 62–67.

[3] P. Pillay and R. Krishnan, "Modeling, simulation, and analysis of permanent-magnet motor drives. i. the permanent-magnet synchronous motor drive," *Industry Applications, IEEE Transactions on*, vol. 25, no. 2, pp. 265–273, 1989.

[4] S.-i. Sakai, H. Sado, and Y. Hori, "Motion control in an electric vehicle with four independently driven in-wheel motors," *Mechatronics, IEEE/ASME Transactions on*, vol. 4, no. 1, pp. 9–16, 1999.

[5] J. Kim and H. Kim, "Electric vehicle yaw rate control using independent in-wheel motor," in *2007 Power Conversion Conference-Nagoya*, 2007, pp. 705–710.

[6] C. Geng, L. Mostefai, M. Denaï, and Y. Hori, "Direct yaw-moment control of an in-wheel-motored electric vehicle based on body slip angle fuzzy observer," *Industrial Electronics, IEEE Transactions on*, vol. 56, no. 5, pp. 1411–1419, 2009.

[7] D. Kim, S. Hwang, and H. Kim, "Vehicle stability enhancement of four-wheel-drive hybrid electric vehicle using rear motor control," *Vehicular Technology, IEEE Transactions on*, vol. 57, no. 2, pp. 727–735, 2008.

[8] J. Kim, C. Park, S. Hwang, Y. Hori, and H. Kim, "Control algorithm for an independent motor-drive vehicle," *Vehicular Technology, IEEE Transactions on*, vol. 59, no. 7, pp. 3213–3222, 2010.

[9] F. J. Perez-Pinal, I. Cervantes, and A. Emadi, "Stability of an electric differential for traction applications," *Vehicular Technology, IEEE Transactions on*, vol. 58, no. 7, pp. 3224–3233, 2009.

[10] Y. Chen and J. Wang, "Design and evaluation on electric differentials for overactuated electric ground vehicles with four independent in-wheel motors," *Vehicular Technology, IEEE Transactions on*, vol. 61, no. 4, pp. 1534–1542, 2012.

[11] M. Lobur, Y. Darnobyt, and R. Kryvyy, "Methods of car speed measurement based on doppler's effect," in *CAD Systems in Microelectronics (CADSM), 2011 11th International Conference The Experience of Designing and Application of*. IEEE, 2011, pp. 394–396.

[12] L. Cocco and S. Rapuano, "Accurate speed measurement methodologies for formula one cars," in *Instrumentation and Measurement Technology Conference Proceedings*, 2007, pp. 1–6.

[13] K. Kobayashi, K. C. Cheok, and K. Watanabe, "Estimation of absolute vehicle speed using fuzzy logic rule-based kalman filter," in *American Control Conference, Proceedings of the 1995*, vol. 5. IEEE, 1995, pp. 3086–3090.

[14] H. Fujimoto, A. Tsumasaka, and T. Noguchi, "Direct yaw-moment control of electric vehicle based on cornering stiffness estimation," in *Industrial Electronics Society, 2005. IECON 2005. 31st Annual Conference of IEEE*. IEEE, 2005, pp. 6–pp.